Progress In Electromagnetics Research, PIER 64, 257–278, 2006

EFFECT OF ANTENNA ARRAY GEOMETRY AND ULA AZIMUTHAL ORIENTATION ON MIMO CHANNEL PROPERTIES IN URBAN CITY STREET GRID

A. A. Abouda, H. M. El-Sallabi, and S. G. Häggman

Helsinki University of Technology
P.O. Box 3000, FIN-02015 HUT, Finland

Abstract—Propagation environment and antenna array configuration have significant effect on spatial correlation properties of multiple-input multiple-output (MIMO) wireless communications channels. In this paper the effect of different antenna array geometries on MIMO channel properties is investigated in urban city street grid propagation environment. Four antenna array geometries with the same number of antenna elements and fixed inter-element spacing are considered, namely, uniform linear array (ULA), uniform circular array (UCA), uniform rectangular array (URA) and uniform cubic array (UCuA). The effect of ULA orientation in azimuthal plane on MIMO channel ergodic capacity is also investigated. Varying orientation angle from 0 to π at the two communication ends is considered. The investigation is carried out based on three dimensional (3D) spatial multi-ray realistic propagation channel model covering different propagation types. It is shown that the antenna array geometry have significant impact on MIMO channel properties. Under different propagation scenarios the ULA shows superiority to the other considered geometries in terms of the ergodic channel capacity and number of spatial parallel channels. However, this superiority depends largely on the array azimuthal orientation.

1. INTRODUCTION

More services and higher data rates are the demands of future wireless communication system end users. In order to accommodate these expectations while maintaining robustness against wireless impairments, contemporary technologies have to be developed. Multiple-input multiple-output (MIMO) techniques stand as a strong candidate to allow robustness against channel fading and interference

as well as to enable high data rates [1, 2]. However, the performance of future MIMO wireless communication systems strongly depends on the propagation environment and the antenna array configuration [3][4]. Previous research results have focused largely on evaluating MIMO system performance under the assumption of uniform linear array (ULA) geometry at both ends with a specific array orientation. Despite the implementation advantages of other array geometries, they have not been extensively investigated. Recently, in [5] the impact of five antenna array geometries on wireless MIMO system performance has been studied using the clustered channel model [6] in indoor scenario. It is shown in [5] that in low spatial correlation environment the ULA geometry outperforms the other considered array geometries in terms of channel capacity and bit error rate performance. In [7] a compact MIMO antenna array was proposed by combining polarization diversity and space diversity into one arrangement consisting of a cube. It is shown that even for very small inter-element spacing considerable capacity is obtained due to polarization diversity.

The assumption of a specific array orientation at both of the transmitter and the receiver ends requires the arrays at the two ends to be fixed to a specific direction. In reality, this is a valid assumption for fixed wireless communications systems but in mobile communications fixed array orientation at base station (BS) side is a realistic assumption meanwhile it is not in the mobile side. The mobile station (MS) is unlikely to be fixed to a specific direction. The effect of azimuthal array orientation on MIMO system performance has been studied in [8] and [9]. In [8] it is shown that the maximum channel capacity is obtained when the ULA at the two communication ends are 'broadside' orientated to each other. However, their investigation was carried out based on a stochastic channel model [10]. In [9] based on data measured in an office corridor it is shown that under line-of-sight (LOS) conditions the channel capacity varies significantly depending on the receiver array orientation. However, due to cost and complexity of field measurements only a few array orientation angles at the receiver side were considered.

The performance of MIMO wireless communication systems highly depends on the propagation environment, antenna array geometry and the antenna element properties. In previous work we have studied the influence of environment physical parameters on the capacity of outdoor MIMO channel [11]. Parameters such as street width, wall relative permittivity and reflection order were considered. In this paper we present detailed investigation on the effect of antenna array geometry and ULA azimuthal orientation on outdoor MIMO channel properties. Four antenna array geometries with eight antenna elements

and fixed inter-element spacing are considered, namely, uniform linear array, uniform circular array (UCA), uniform rectangular array (URA) and uniform cubic array (UCuA). The effect of antenna array geometry on MIMO channel properties is studied by analyzing the eigenvalues of the normalized channel correlation matrix. To study the effect of ULA azimuthal orientation on MIMO channel properties, the obtained ergodic channel capacity with different array orientation angles at both ends is analyzed. The investigation is carried out in outdoor microcellular environment using a three dimensional (3D) deterministic propagation channel model based on electromagnetic theory. Results for different propagation types are presented and analyzed.

The rest of this paper is organized as follows: The considered antenna array geometries and the ULA azimuthal orientation are presented in Section 2. The propagation channel model utilized in this study is described in Section 3. The eigenvalues and the channel capacity calculations are presented in Section 4. Numerical results and intuitive discussions are given in Section 5. Our conclusions are drawn in Section 6.

2. ARRAY GEOMETRIES AND ULA AZIMUTHAL ORIENTATION

Fig. 1 depicts the considered antenna array geometries and shows the reference azimuthal orientation angle of each geometry. All the orientation angles are calculated relative to the x-axis (0°) with anti-

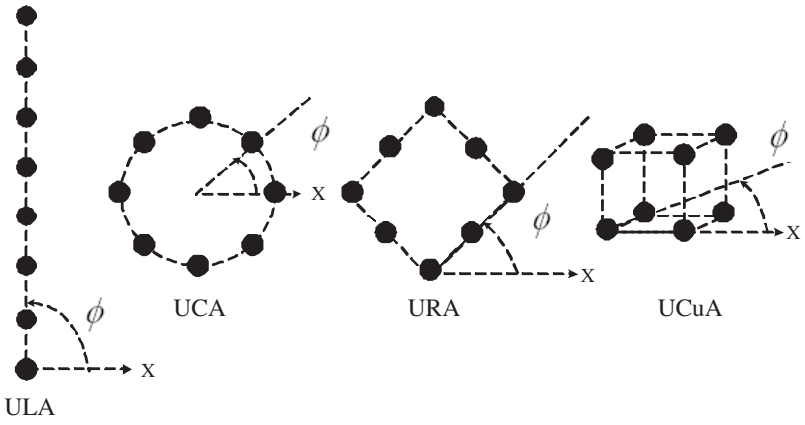

Figure 1. Considered antenna array geometries and reference azimuthal orientation angle ϕ.

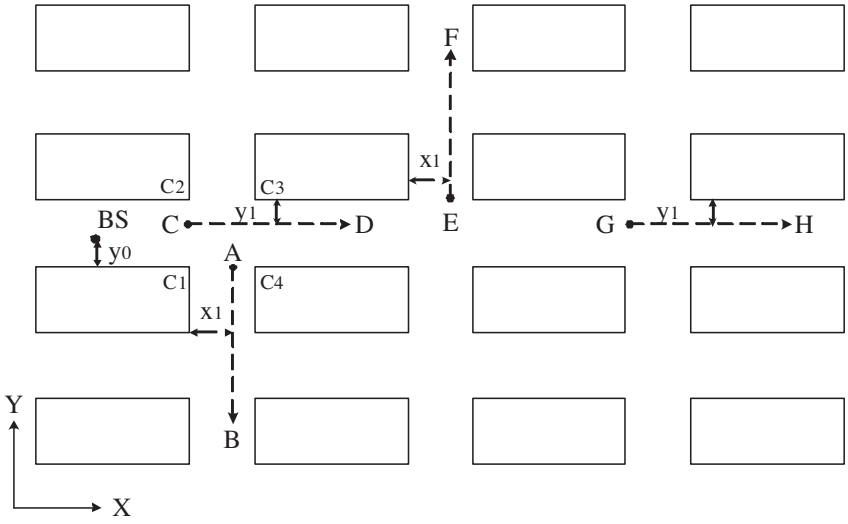

Figure 2. Urban street grid showing traveling routes under study.

clock wise rotation. Each geometry has eight antenna elements that is distributed in an uniform shape. These geometries represent three types of antenna arrays, one dimensional ULA, two dimensional UCA and URA and three dimensional UCuA. In principle the antenna elements could be of different field pattern, polarization and inter-element spacing, however, in this study we consider omnidirectional radiation patterns and vertical polarization with 0.5λ inter-element spacing, where λ is the wavelength.

This study is conducted in one of the typical deployment scenarios defined in standardization [12] and is shown in Fig. 2. Typical traveling routes that represent different propagation scenarios in urban microcellular environment are considered, namely, traveling route A-B, C-D, E-F and G-H. The different antenna array geometries are deployed at both ends and the eigenvalues of the normalized channel correlation matrix are computed in each traveling route under fixed array orientation. Later the effect of ULA orientation angle in azimuthal plane on the ergodic channel capacity is studied on the same traveling routes by computing the ergodic channel capacity under different ULA azimuthal orientation angles at both ends. The effect of the azimuthal array orientation on the performance of the other array geometries is not considered in this work. However, it should be noticed that the results obtained from the ULA azimuthal orientation studies can be projected into the performance of the other geometries.

3. UTILIZED CHANNEL MODEL DESCRIPTION

Successful design and deployment of MIMO wireless communication systems require detailed channel characterization. In order to carry out this characterization, two approaches are widely common, field measurements, e.g., [13], and model-based, e.g., [14]. The field measurement is costly, time consuming, the results are site dependent and it also requires skilled personnel. Due to the difficulties of field measurement-based characterization, many researchers have turned to model-based characterization approach. The advantage of model based analysis is the flexibility of testing the influence of different parameters that can not be controlled in field measurements in addition to the possibility of interpreting the obtained results more accurately.

A three dimensional (3D) spatial variant multi-ray radio wave propagation models for main street and perpendicular streets in an urban street grid were developed in [15] and [16], respectively. The propagation channel models are different from ray tracing models in a sense that there is no searching for coupling paths between BS and MS since all the ray characteristics, such as angle of arrival (AOA), angle of departure (AOD) and path length, are given in closed form mathematical expressions by using the set membership criteria. The advantage of getting the ray characteristics in explicit mathematical expressions is significant reduction in computation time which is the main limitation of the available simulation tools. Performing this study based on field measurement is costly and complex in terms of design and implementation of different antenna array geometries and orientation. Therefore, these propagation channel models are adopted to carry out this study.

For MIMO channels, the complex channel gain between jth transmit antenna element and ith receive antenna element is given by [15, 16]:

$$g_{V,H}(i,j) = g_{V,H}^{RR}(i,j) + g_{V,H}^{RDR}(i,j) \tag{1}$$

where $g_{V,H}^{RR}$ and $g_{V,H}^{RDR}$ are the total complex channel gain due to reflected-reflected (RR) rays group and reflected-diffracted-reflected (RDR) rays group, respectively, with transmission in vertical polarization (VP) and horizontal polarization (HP), respectively.

The complex channel gain of the RR rays and the RDR rays are given by [16]:

$$g_{V,H}^{RR}(i,j) = \frac{\lambda}{4\pi} \sum_{k\equiv(m,s,n,u,g)} \frac{1}{r_k(i,j)} f_{BS}(\vartheta_k,\varphi_k)(\mathcal{R}_{V,H}^{k}(i,j))^g \\ (R_{H,V}^{kn}(i,j))^n (R_{H,V}^{km}(i,j))^m f_{MS}(\theta_k,\phi_k) e^{(\frac{-j2\pi}{\lambda} r_k(i,j))} \tag{2}$$

and

$$g_{V,H}^{RDR}(i,j) = \frac{\lambda}{4\pi} \sum_{k\equiv(m,s,n,u,g,C_k)} f_{BS}(\vartheta_k,\varphi_k)(\mathcal{R}_{V,H}^{k}(i,j))^{g}(R_{kH,kV}^{kn}(i,j))^{n} \frac{(R_{H,V}^{km}(i,j))^{m}\mathcal{D}_{H,V}^{k}(i,j)f_{MS}(\theta_k,\phi_k)e^{(\frac{-j2\pi}{\lambda}(D_1(i,j)+D_2(i,j)))}}{\sqrt{D_1(i,j)D_2(i,j)(D_1(i,j)+D_2(i,j))}} \tag{3}$$

where each ray k is represented by a set of five integers (m, s, n, u, g) which characterize ray k, m and n are the wall reflection orders in the main street and perpendicular streets, respectively, $s = 1, 2$ and $u = 1, 2$ are for two sidewalls on the street for BS and MS, respectively, $g = 0, 1$ is for the ground reflection, when $m = 0$, $s = 0$, $u = 0$ ray k is characterized by g, if $g = 0$, ray k is the LOS path and if $g = 1$ ray k is paired ground reflection path, r_k is the path length, $f_{BS}(\vartheta, \varphi)$ and $f_{MS}(\theta, \phi)$ are the BS and MS antenna field patterns with polarization information, respectively, (ϑ_k, φ_k) and (θ_k, ϕ_k) are the elevation and azimuth AOD and AOA for the kth ray at BS and MS, respectively, $\mathcal{R}_{V,H}^{k}$, $R_{H,V}^{km}$ and $R_{H,V}^{kn}$ are the well-known Fresnel reflection coefficients for ground and wall reflections in main and perpendicular streets, respectively, with transmission in VP and HP, respectively, $\mathcal{D}_{H,V}^{k}$ is the diffraction coefficient at the vertical edge of the building corner with transmission in VP and HP, respectively, $D_{1,2}$ is the distance from the BS and the MS to the diffraction point, respectively, $C_{1,2,3,4}$ are four building corners.

For a MS located at (x,y) with antenna height h_m, the path length of the kth ray that couples the MS to a BS located at (0,0) with antenna height h_B is given by [16]:

$$r_k = \sqrt{\begin{array}{l}((n+(-1)^{u}\Xi(n))w_2+(-1)^{u}(x-2\Xi(n)x_1))^2 \\ +((-1)^{s}((m+(-1)^{s}\Pi(m))w_1-2(-1)^{s}\Xi(m)y_1)-y)^2 \\ +(h_B-(-1)^{g}h_m)^2\end{array}} \tag{4}$$

where

$$\Xi(\chi) = \begin{cases} 1, & \forall \quad \chi \quad \text{even} \\ 0, & \forall \quad \chi \quad \text{odd} \end{cases} \tag{5}$$

w_1 and w_2 are widths of the main and perpendicular streets, x_1 and y_1 are the distances shown in Fig. 2. The azimuthal AOD and AOA of the kth ray are given by [16]:

$$\varphi_k = \arctan\left(\frac{(-1)^{m}\text{sgn}(y)((m-\text{sgn}(y)\Xi(m))w_1+2\text{sgn}(y)\Xi(m)y_1+|y|)}{(-1)^{u}((n+(-1)^{u}\Xi(n))w_2+(-1)^{u}(x-2\Xi(n)x_1))}\right) \tag{6}$$

$$\phi_k = \arctan\left(\frac{(-1)^s((m+(-1)^s\Xi(m))w_1 - 2(-1)^s\Xi(m)y_1) - y}{(-1)^{n+1}((-1)^u((n+\Xi(n))w_2 - 2\Xi(n)x_1) + x)}\right) \quad (7)$$

where arctan(.) returns the angle in the corresponding quadrant. More details can be found in [15] and [16].

4. EIGENVALUES AND CHANNEL CAPACITY CALCULATIONS

The eigenvalue decomposition of the instantaneous channel correlation matrix is a useful tool for MIMO system performance investigation. The distribution of the eigenvalues of the channel correlation matrix reveals valuable information about the MIMO channel properties and consequently predicts the MIMO system performance. While the number of the non zero eigenvalues reflects the spatial multiplexing gain [17] that can be obtained over a given channel, the eigenvalues represent the power gain [18] in each spatial channel. The eigenvalues are obtained by applying the eigenvalue decomposition on the channel correlation matrix as follows:

$$\lambda_i = \text{EVD}(\mathbf{H}\mathbf{H}^H), \quad i = 1, 2, ..., R(\mathbf{H}\mathbf{H}^H) \quad (8)$$

where $\mathbf{H} \in C^{N_r, N_t}$ is the normalized channel matrix with N_t transmit antennas and N_r receive antennas, λ_i is the ith eigenvalue of the channel correlation matrix, EVD($\mathbf{A}$) returns the eigenvalues of matrix $\mathbf{A}$ and $R(\mathbf{A})$ denotes the rank of matrix $\mathbf{A}$.

The channel capacity under fixed average receive signal to noise ratio (SNR) is usually used as a performance measure of MIMO systems. It maps the eigenvalues of the channel correlation matrix to a single number that can be used for easy benchmark. Under spatial multiplexing scheme [19] and with equal power allocation strategy, the channel capacity will be the sum of the capacities supported by each spatial subchannel. Therefore, the total channel capacity at each channel realization can be written as [18]:

$$c = \sum_{i=1}^{R(\mathbf{H}\mathbf{H}^H)} \log\left(1 + \lambda_i \frac{\rho}{N_t}\right) \quad \text{b/s/Hz} \quad (9)$$

where ρ is the average receive SNR.

5. RESULTS AND DISCUSSIONS

5.1. Simulation Environment and Parameters

The geometry of the urban microcellular environment under study is depicted in Fig. 2 where the street grid pattern has 100 m × 50 m blocks of building and 25 m street widths for the main street, where the BS is located, and perpendicular streets. The building street surface electrical parameters are relative permittivity $\epsilon_r = 5$ and conductivity $\sigma = 0.005\,\mathrm{S/m}$. These are practical values for city street concrete walls [20]. The environment multipath richness, from channel modeling perspective, is a function of the maximum reflection orders in the main and perpendicular streets. Since one reflection results in about 5 dB loss, rays reflected more than 7 times are very weak [11]. Therefore, the maximum reflection order is set to 7 in both main and perpendicular streets. The BS is mounted below the rooftops with antenna height 13 m at distances of 75 m from corner C_1 and 5 m from the wall, $y_1 = 5\,\mathrm{m}$. A MS with antenna height 1.8 m moves a distance of 100 m in each traveling route with $x_1 = 13\,\mathrm{m}$ and $y_1 = 5\,\mathrm{m}$.

In the following numerical results a carrier frequency of 2 GHz is assumed. Throughout the traveling routes, channel realizations are computed every 10 cm. The channel capacity calculations are performed at 20 dB average receive SNR.

5.2. Traveling Routes Description

It is widely known that the performance of wireless MIMO communication systems depends on the dominant propagation mechanism [21] and the propagation environment geometry [22]. The traveling routes under study represent different propagation types and there are different dominant propagation mechanisms throughout the routes. For instance, traveling route A-B is a non line of sight (NLOS) scenario. The dominant propagation mechanism in this route changes with the MS location. At the beginning of the route there is a strong LOS component due to the presence of the direct path and its ground reflected pair. The LOS component disappears when the MS moves inside the perpendicular street. Then the environment will be dominated by the reflection mechanism. As the MS goes inside the perpendicular street the RR rays group will suffer from high attenuation due to multiple reflections and the diffraction mechanism will become more dominant. At the end of the route the RR rays group will vanish and only RDR rays group will be available. Most of the dominant RDR rays group will be due to the signal diffracted from corner C_3, (see Fig. 2), which results in a scenario similar to

low k-facor situation though it is NLOS. The propagation scenario in traveling route E-F is NLOS where both RR rays group and RDR rays group are available but the RR rays group exist for short distances of the route due to large separation distance between BS and MS. Most of the dominant RDR rays group in this route will be due to the signal diffracted from corner C_4 in the second crossing perpendicular street. On the other hand, traveling routes C-D and G-H are LOS scenarios. Throughout the routes the direct ray and its ground reflected pair and the two sidewalls reflected rays are the dominant propagation components. In traveling route G-H the separation distance between the BS and the MS is larger than that of route C-D. This results in a LOS scenario with low angular spread (AS) compared to route C-D. In this case the channel matrix will be dominated by the direct path and its ground reflected pair.

5.3. Effect of Antenna Array Geometry on MIMO Channel Eigenvalues

The different antenna array geometries are deployed at both ends and the channel matrices are computed in each traveling route. Fixed array orientation for the all considered geometries is assumed. Orientation angle, $\phi = 0$, at both ends for the UCA, URA and the UCuA is assumed. For the ULA broadside array orientation is assumed for the BS array, ϕ_{BS}=$\pi/2$. In the MS side two possible ULA orientations are considered; 1)- Transversal to the main street for routes C-D and G-H, $\phi_{MS} = \pi/2$, 2)- Transversal to the perpendicular street for routes A-B and E-F, $\phi_{MS} = 0$.

5.3.1. Eigenvalues Analysis

Figs. 3 and 4 show the effect of different antenna array geometries on the eigenvalues of MIMO channel at 10% outage probability in LOS traveling routes, C-D and G-H, respectively. The power gain distribution of single input single output (SISO) system arbitrarily chosen from each of the obtained channel matrices is calculated and denoted as γ_S. In addition, the power gain distribution in the case of SISO system with Rayleigh distribution is also calculated and denoted as γ_R. Both γ_S and γ_R serve as references in the following discussions. It can be noticed that in both traveling routes $\gamma_S > \gamma_R$ which is the case of Ricean channel when there is a strong LOS component. In terms of the number of parallel channels, using the ULA results in four parallel channels with $\lambda_i \geq \gamma_S$ available 90% of the time in traveling route C-D. These parallel channels are capable of carrying high data rates to the receiver. In traveling route G-H the number of significant parallel

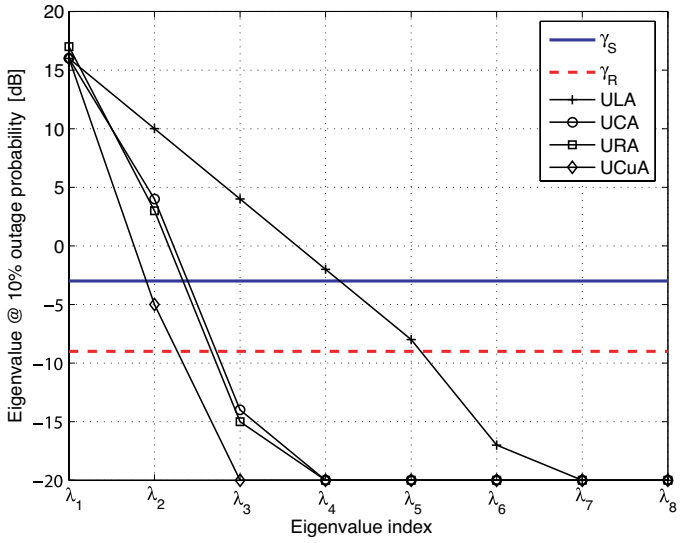

Figure 3. Eigenvalues of channel correlation matrix read at 10% outage probability in traveling C-D.

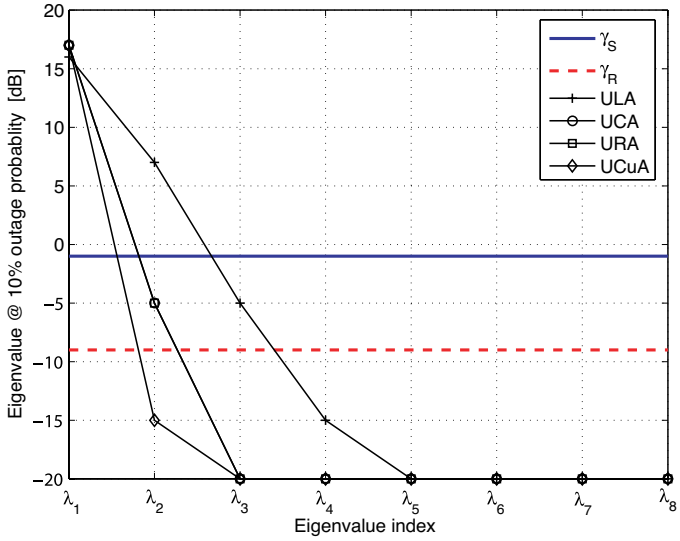

Figure 4. Eigenvalues of channel correlation matrix read at 10% outage probability in traveling G-H.

channels reduces to two due to the lower AS. The UCuA maintains only one significant channel in both routes since only one eigenvalue is larger than γ_S. Because the second eigenvalue in traveling route C-D, λ_2, is higher than that in traveling route G-H, higher channel capacity can be obtained in traveling route C-D with UCuA. The use of UCA and URA geometries have similar impact on the MIMO channel eigenvalues in both routes where the available significant channels in traveling routes C-D and G-H are two and one, respectively.

The eigenvalues of the channel correlation matrix at 10% outage probability in NLOS traveling routes, A-B and E-F, are shown in Figs. 5 and 6, respectively. In these scenarios γ_S is close to γ_R in both routes which means that the amplitude of channel matrix elements can be closely modeled as Rayleigh distributed random variable. However, there are some dominant reflected components that result in Ricean channel with low k-factor. Using ULA, UCA or URA in traveling route A-B results in four, three and three parallel channels with $\lambda_i \geq \gamma_S$ available 90% of the time, respectively. When the UCuA is deployed, only two significant parallel channels are available which reduces the achievable data rate significantly. Similar observations are made in traveling route E-F, where there are three parallel channels available by using ULA, UCA and URA while using the UCuA results in two parallel channels.

5.3.2. Insight View of Antenna Array Geometry Effect

It can be observed that the performance of the different antenna array geometries depends on the number of array elements facing the direction of wave propagation and the distance between these elements. In the case of ULA geometry, the number of elements facing the direction of wave propagation is eight with inter-element spacing 0.5λ, while in the UCA and the URA geometries the number of elements facing the direction of wave propagation are five, (half of the circle), and three, (one side of the rectangle), respectively, with real inter-element spacing $<0.5\lambda$ and 0.5λ, respectively. For the UCuA geometry, the inter-element spacing is 0.5λ with four elements facing the direction of wave propagation, (one side of the cube). The UCuA has two layers, upper layer and lower layer. The four elements in the upper layer and the four elements in the lower layer will have highly correlated signals because the radio wave propagation takes place in horizontal plane in the considered propagation environment. This will reduce the number of effective antenna elements facing the wave propagation direction to about two. Therefore, distributing the antenna elements in three dimensions does not seem attractive in low elevation angle spread propagation environment. It should be noticed

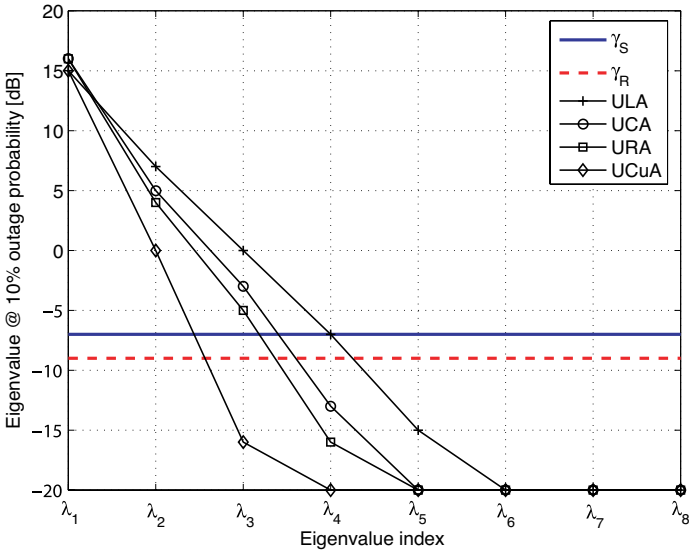

Figure 5. Eigenvalues of channel correlation matrix read at 10% outage probability in traveling A-B.

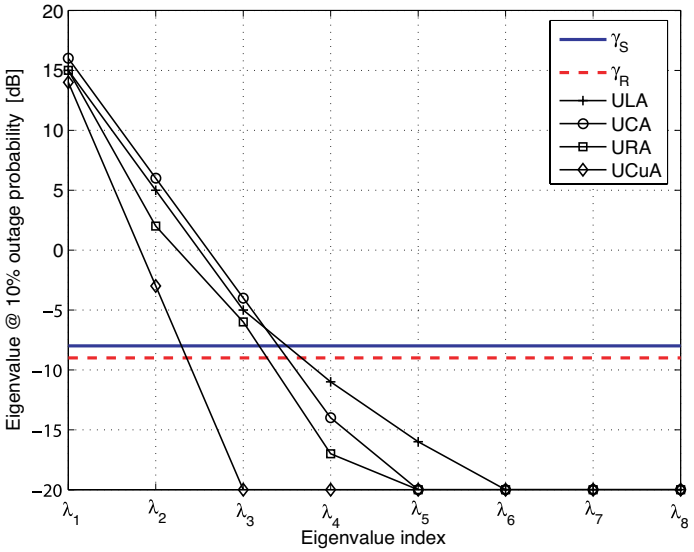

Figure 6. Eigenvalues of channel correlation matrix read at 10% outage probability in traveling E-F.

that in indoor propagation environment the three dimensional antenna array geometry may benefit from the ceiling and back reflected signals.

5.4. Effect of ULA Azimuthal Orientation on MIMO Channel Ergodic Capacity

In spite of the geometrical simplicity of the ULA, it has shown superiority to other considered geometries in terms of the number of parallel channels under different propagation scenarios. However, this superiority is valid only under some specific array orientation angles. In this section varying ULA orientation angle from 0 to π at the two communications ends is considered with step sizes of $\pi/4$ and $\pi/8$ for the BS array (ϕ_{BS}), and the MS array (ϕ_{MS}), respectively.

5.4.1. Ergodic Channel Capacity Analysis

The effect of ULA azimuthal orientation at the two communications ends on the ergodic channel capacity in LOS traveling routes, C-D and G-H, are shown in Figs. 7 and 8, respectively. The ergodic channel capacity of SISO channel at the same average SNR, 20 dB, is 6.52 b/s/Hz. The ergodic channel capacity of the SISO channel do not depend on the two ends array orientation angles and it is used as a reference in the following discussions. It is clear that the MIMO channel capacity highly depends on the array orientation angles at the two ends. For instance, in traveling route C-D where the AS is higher than that in route G-H, when the ULA orientation angles $\phi_{BS} = \pi/2$ and $\phi_{MS} = \pi/2$, the MIMO ergodic channel capacity increase relative to the SISO channel is about 22.79 b/s/Hz. Turning the MS orientation angle to 0 or π reduces the relative MIMO ergodic channel capacity gain to 8.51 b/s/Hz.

In low AS propagation scenario, like the case in traveling route G-H, the impact of ULA azimuthal orientation on the MIMO channel capacity performance is evident. With $\phi_{BS} = \pi/2$ and $\phi_{MS} = \pi/2$ the relative MIMO capacity gain is 14.48 b/s/Hz. When the ULA orientation angles at both ends are set to 0 or π, the MIMO channel capacity gain over the SISO channel is only 3 b/s/Hz.

Figs. 9 and 10 show the effect of ULA azimuthal orientation angles at the two ends on MIMO channel ergodic capacity in NLOS traveling routes A-B and E-F, respectively. Deploying the MIMO technique results in relative high and low channel capacity gain over the SISO channel at different ULA orientation angles. For instance, in traveling route A-B the highest relative channel capacity gain, 29.62 b/s/Hz, is obtained when $\phi_{BS} = \pi/4$ and $\phi_{MS} = 3\pi/4$. In traveling route E-F the highest relative channel capacity gain, 26.52 b/s/Hz, is obtained

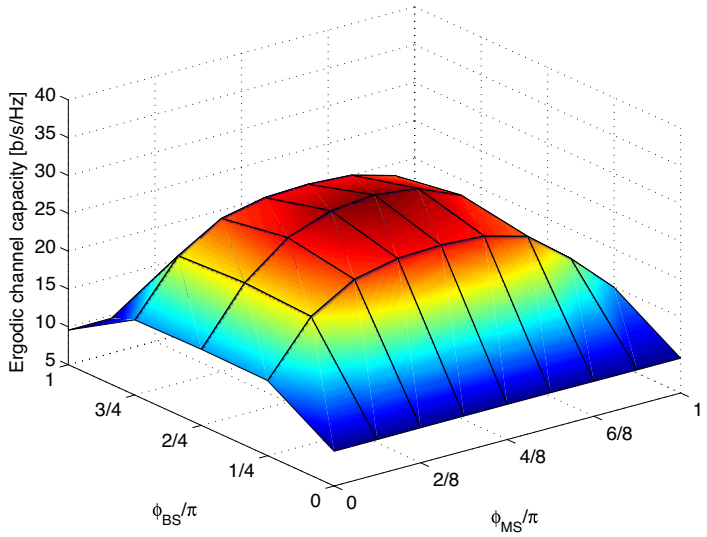

Figure 7. Effect of azimuthal ULA orientation on the ergodic channel capacity in traveling route C-D at 20 dB SNR.

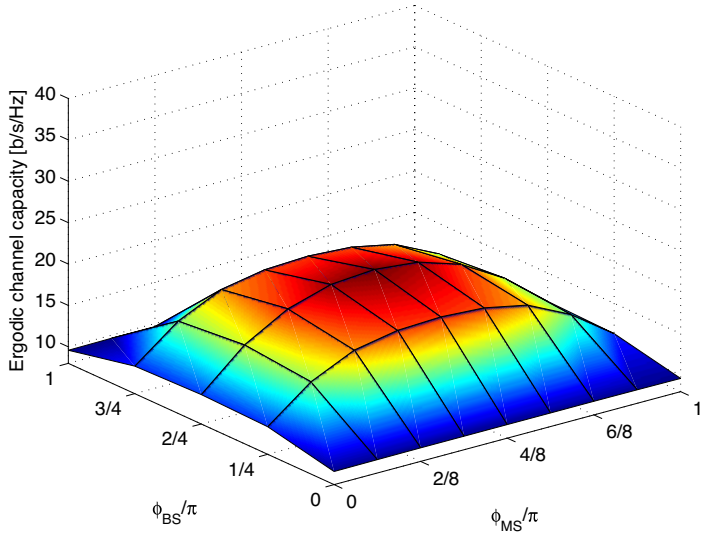

Figure 8. Effect of azimuthal ULA orientation on the ergodic channel capacity in traveling route G-H at 20 dB SNR.

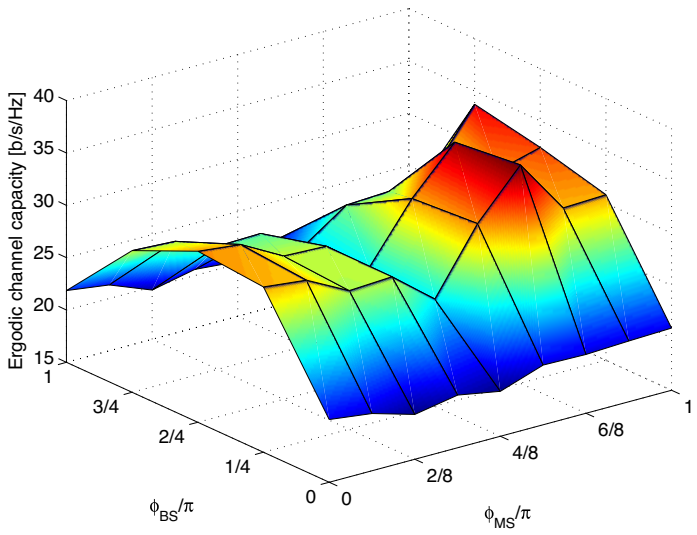

Figure 9. Effect of azimuthal ULA orientation on the ergodic channel capacity in traveling route A-B at 20 dB SNR.

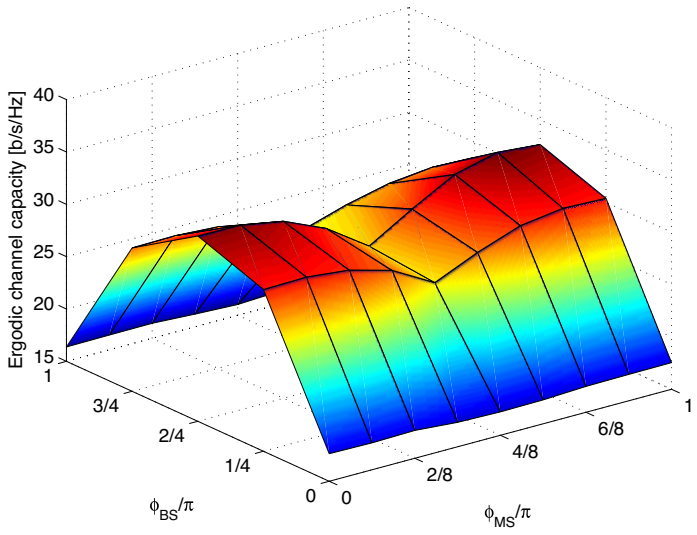

Figure 10. Effect of azimuthal ULA orientation on the ergodic channel capacity in traveling route E-F at 20 dB SNR.

when $\phi_{BS} = \pi/2$ and $\phi_{MS} = 7\pi/8$ or $\phi_{MS} = \pi/8$. However, higher resolution of ϕ_{BS} may result in high relative channel capacity gain at different ϕ_{BS}. Changing the orientation angles to $\phi_{BS} = 0$ or π and $\phi_{MS} = \pi/2$ reduces the relative MIMO channel capacity gain to 13.05 b/s/Hz in traveling route A-B and in traveling route E-F to 11.09 b/s/Hz.

5.4.2. Insight View of ULA Azimuthal Orientation Effect

It can be noticed that in the all considered traveling routes, in order to obtain the highest ergodic channel capacity with ULA geometry, the two communication ends should be turned to face the main direction of the radio wave propagation. This due to the fact that the wave propagation takes place in horizontal plane in the considered scenarios and the resolution of the ULA array is high when it is transversal to the wave propagation direction. Therefore, the ULA azimuthal orientation can be thought of as a mechanical steering to direct the array beam towards the wave propagation direction. In LOS traveling routes the wave propagation direction is parallel to the main street while in NLOS traveling routes the wave is coming through the street crossing. It can be also noticed that when the ULA at BS side is parallel to the wave propagation direction, the orientation angle at the MS side has insignificant impact on the ergodic channel capacity performance in both LOS and NLOS traveling routes. On the other hand, the BS orientation angle has significant impact on the ergodic channel capacity even when the MS is parallel to the wave propagation direction. This is due to the fact that the ergodic channel capacity performance depends on the spatial correlation properties at the two communication ends. Parallel ULA to the wave propagation direction at the BS side results in high spatial correlation and therefore, varying the orientation angle of the MS array will not have noticeable impact on the channel capacity.

In traveling route A-B the four building corners have substantial impact on the channel capacity performance. For instance, in deep shadow region the propagation scenario is dominated by the RDR rays group. The direct diffracted component from corner C_3 is the dominant and other components are so weak with respect to it which results in a situation with low k-factor. As we have seen, the highest channel capacity is obtained when the two communications ends are transversal to the wave propagation direction, in traveling route A-B, the highest channel capacity is obtained when the array at the MS side is transversal to corner C_3 which can be considered as a secondary source. In BS side three orientation angles result in high relative channel capacity gain, $\phi_{BS} = 3\pi/4$, $\phi_{BS} = \pi/2$ and $\phi_{BS} = \pi/4$.

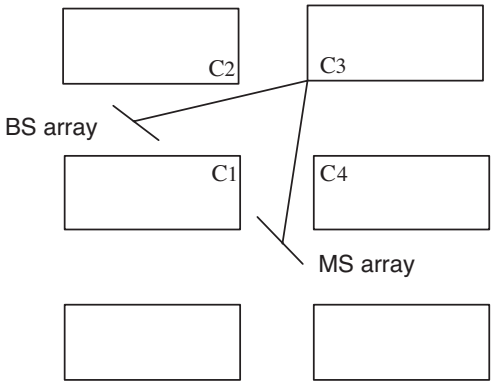

Figure 11. Illustration of corner C_3 role on the effect of ULA azimuthal orientation in traveling route A-B.

Illustration of corner C_3 role on the effect of array orientation in traveling route A-B when $\phi_{BS} = 3\pi/4$ and $\phi_{MS} = 3\pi/4$ is shown in Fig. 11 where the two communications ends face the diffraction corner C_3. However, the positions of the two communications ends and the separation distance between them have influence on the resolution of the array orientation. In traveling route E-F, it can be noticed that the array resolution to the orientation angles is less than that in traveling route A-B due to separation distance. This piece of information might be very valuable for fixed wireless communications systems deployment. In order to achieve maximum channel capacity in NLOS scenarios, our findings suggest taking into account the geometry of the propagation environment when installing the antenna arrays at both ends.

5.5. Comparison of channel capacity performance

Figs. 12, 13, 14 and 15 show the cumulative distribution function (CDF) of the channel capacity obtained with different antenna array geometries in traveling routes A-B, C-D, E-F and G-H, respectively, at 20 dB average SNR. The channel capacity obtained under the assumption of independent identical distributed (iid) complex Gaussian elements with the same MIMO system size and at the same average SNR is also shown in these figures. In practice, the MS orientation angle is unlikely to be fixed to a specific direction but the BS array most probably going to be fixed. Therefore, the channel capacity performance of the ULA is shown for three cases; 1)- averaging over all orientation angles at both ends, denoted as ULA, 2)- averaging

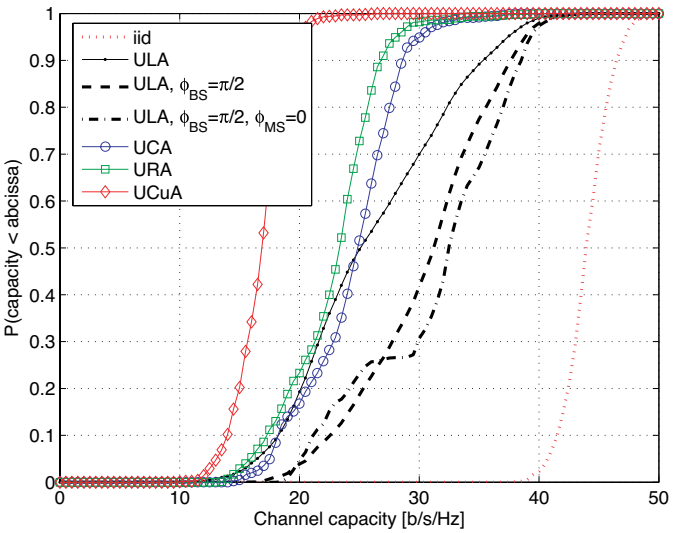

Figure 12. CDFs of channel capacity obtained with different antenna array geometries at 20 dB SNR in traveling route A-B.

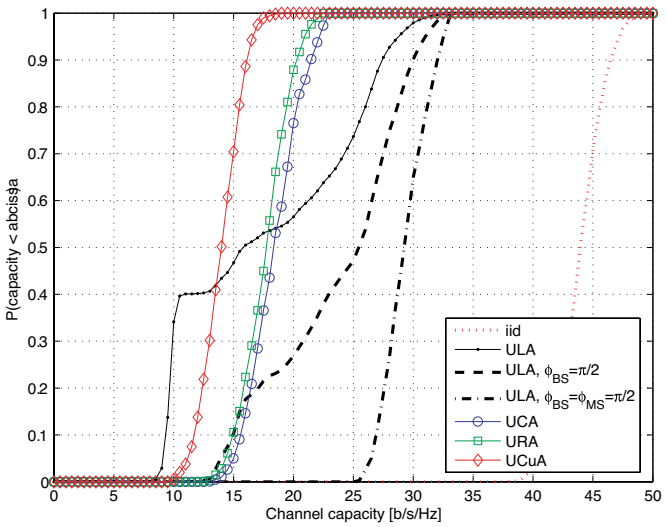

Figure 13. CDFs of channel capacity obtained with different antenna array geometries at 20 dB SNR in traveling route C-D.

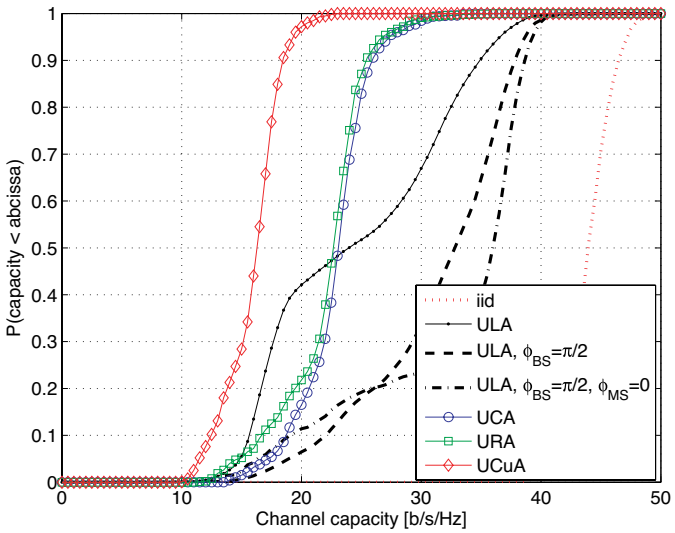

Figure 14. CDFs of channel capacity obtained with different antenna array geometries at 20 dB SNR in traveling route E-F.

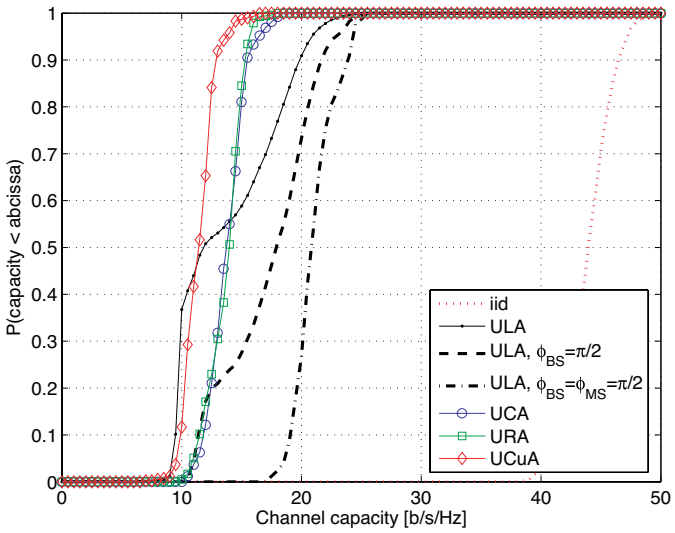

Figure 15. CDFs of channel capacity obtained with different antenna array geometries at 20 dB SNR in traveling route G-H.

over all MS orientation angles with fixed BS array, $\phi_{BS} = \pi/2$ and 3)-fixed array orientation angle at both ends, $\phi_{BS} = \pi/2$ and $\phi_{MS} = 0$ in NLOS traveling routes, A-B and E-F and $\phi_{MS} = \pi/2$ for LOS traveling routes C-D and G-H. It can be noticed that in these propagation scenarios the maximum achievable channel capacity, regardless of the antenna array geometry, is less than that of the iid channel. This is due to the fact that the iid assumption requires rich scatter environment which is not the case in the propagation environment under study. It can be clearly seen that in general the ULA outperforms the other geometries in terms of channel capacity performance even when the BS array is not assumed fixed. However, fixing the BS array to $\phi_{BS} = \pi/2$ improves the channel capacity performance significantly relative to the case where both ends are not assumed fixed. In NLOS traveling routes A-B and E-F the relative increase in the median channel capacity is about 6 and 7 b/s/Hz, respectively, while in LOS traveling routes C-D and G-H the relative increase in the median channel capacity is about 9 and 6 b/s/Hz, respectively. However, keeping the BS array fixed to $\phi_{BS} = \pi/2$ and turning the MS array to $\phi_{MS} = \pi/2$ in traveling routes C-D and G-H or to $\phi_{MS} = 0$ in traveling routes A-B and E-F also results in significant increase in channel capacity performance compared to the case when only fixed BS array is assumed. This relative increase ranges from 1.3 b/s/Hz in traveling route A-B to 4 b/s/Hz in traveling route C-D.

6. CONCLUSIONS

We have shown that antenna array geometry and ULA azimuthal orientation have significant impact on MIMO channel properties. It is concluded that the MIMO channel properties highly depends on the number of antenna array elements facing the wave propagation direction and the distance between these elements. In outdoor microcellular environment under LOS and NLOS propagation conditions the ULA outperforms the other array geometries in terms of the number of significant parallel channels and the ergodic channel capacity. Since specific array orientation at BS side is an engineering choice, the obtained results suggest that using ULA to obtain the maximum channel capacity, the BS array should be transversal to the main direction of the LOS and NLOS propagation.

REFERENCES

1. Foschini, G. J. and M. J. Gans, "On limits of wireless communications in a fading environment when using multiple antennas," *Wireless Personal Commun.*, Vol. 6, No. 3, 311–335, 1998.
2. Telatar, I. E., "Capacity of multi-antenna Gaussian channels," *European Trans. Tel.*, Vol. 10, No. 6, 585–595, 1999.
3. Shui, D. S., G. J. Foschini, M. J. Gans, and J. M. Kahn, "Fading correlation and its effect on the capacity of multielement antenna systems," *IEEE Trans. on Commun.*, Vol. 48, No. 3, 502–513, 2000.
4. McNamara, D. P., M. A. Beach, and P. N. Fletcher, "Spatial correlation in indoor MIMO channels," *Proc. of IEEE Personal Indoor and Mobile Radio Communications*, Vol. 1, 290–294, 2002.
5. Forenza, A. and R. W. Heath Jr., "Impact of antenna geometry on MIMO communication in indoor clustred channels," *Proc. of IEEE Antennas and Propagation Symposium*, Vol. 2, 1700–1703, 2004.
6. Saleh, A. A. M. and R. A. Valenzuela, "A statistical model for indoor multipath propagation," *IEEE Journal on Selected Areas in Commun.*, Vol. 5, No. 2, 128–137, 1987.
7. Andersen, J. B. and B. N. Getu, "The MIMO cube — a compact MIMO antenna," *Proc. of IEEE Wireless Personal Multimedia Commun.*, Vol. 1, 112–114, 2002.
8. Li, X. and Z. Nie, "Effect of array orientation on performance of MIMO wirelss channels," *IEEE Antenna and Propagation Letters*, Vol. 3, 368–372, 2004.
9. Almers, P., F. Tufvesson, P. Karlsson, and A. F. Molisch, "The effect of horizontal array orientation on MIMO channel capacity," *Proc. of IEEE Vehicular Technology Conference VTC03*, 34–38, 2003.
10. Kermoal, J. P., L. Schumacher, K. I. Pedersen, P. E. Mogensen, and F. Frederiksen, "A stochastic MIMO radio channel model with experimental validation," *IEEE Journal on Selected Areas in Commun.*, Vol. 20, No. 6, 1211–1226, 2002.
11. Abouda, A. A, N. G. Tarhuni, and H. M. El-Sallabi, "Model-based investigation on MIMO channel capacity in main street of urban microcells," *Proc. of IEEE Antennas and Propagation Symposium*, 313–316, 2005.
12. TR 101 112 V3.2.0 (1998-04) Technical Report: Universal Mobile Telecommunications System (UMTS); Selection procedures for the

choice of radio transmission technologies of the UMTS (UMTS 30.03 version 3.2.0)

13. Gans, M. J., N. Amitay, Y. S. Yeh, H. Xu, T. C. Damen, R. A. Valenzuela, T. Sizer, R. Storz, D. Taylor, W. M. MacDonald, C. Tran, and A. Adamiecki, "Outdoor BLAST measurement system at 2.44 GHz: calibration and initial results," *IEEE Journal on Selected Areas in Commun.*, Vol. 20, No. 3, 570–583, 2002.
14. Gesbert, D., H. Bolcskei, D. Gore, and A. Paulraj, "Outdoor MIMO wireless channels: models and performance prediction," *IEEE Trans. on Commun.*, Vol. 50, 1926–1934, 2002.
15. El-Sallabi, H. M. and P. Vainikainen, "Physical modeling of line-of-sight wideband propagation in a city street for microcellular communications," *Journal of Electromagnetic Waves and Applications*, Vol. 14, 905–927, 2000.
16. El-Sallabi, H. M. and P. Vainikainen, "Radio wave propagation in perpendicular streets of urban street grid for microcellular communications. Part I: Channel modeling" *Progress In Electromagnetic Research*, PIER 40, 229–254, 2003.
17. Zheng, L. and D. N. Tse, "Diversity and multiplexing: A fundamental tradeoff in multiple-antenna channels," *IEEE Trans. on Information Theory*, Vol. 49, No. 5, 1073–1096, 2003.
18. Andersen, J. B., "Array gain and capacity for known random channels with multiple element arrays at both ends," *IEEE Journal on Selected Areas in Commun.*, Vol. 18, 2172–2178, 2000.
19. Foschini, G. J., G. D. Golden, R. A. Valenzuela, and P. W. Wolniansky, "Simplified processing for high spectral efficiency wireless communication employing multi-element arrays," *IEEE Journal on Selected Areas in Commun.*, Vol. 17, 1841–1852, 1999.
20. Carl Johnk, T. A., *Engineering Electromagnetic Fields and Waves*, 637, John Wiley and Sons Inc., 1988.
21. Herdin, M., H. Özcelik, H. Hofstetter, and E. Bonek, "Linking reduction in measured MIMO capacity with dominant wave propagation," *Proc. of International Conference on Telecommunications ICT03*, 1526–1530, 2003.
22. Driessen, P. and G. J. Foschini, "On the capacity formula for multiple-input multiple-ouput wireless channels: A geometric interpretation," *IEEE Trans. on Commun.*, Vol. 47, No. 2, 173–176, 1999.